Oxygen potential of hypo-stoichiometric La-doped UO_2

Yoshida, Keita
Faculty of Engineering, Kyushu University

Arima, Tatsumi
Faculty of Engineering, Kyushu University

Inagaki, Yaohiro
Faculty of Engineering, Kyushu University

Idemitsu, Kazuya
Faculty of Engineering, Kyushu University

他

出版情報：Journal of Nuclear Materials. 418 (1/3), pp.22-26, 2011-11. Elsevier B.V.
バージョン：

Oxygen Potential of hypo-stoichiometric La-doped UO_2

Keita Yoshida [a], Tatsumi Arima [a, *], Yaohiro Inagaki[a], Kazuya Idemitsu[a], Masahiko Osaka [b], Shuhei Miwa[b]

[a]*Faculty of Engineering, Kyushu University, 744 Motooka, Fukuoka 819-0395, Japan*

[b]*Japan Atomic Energy Agency, 4002 Narita-cho, Oarai-machi, Higashiibaraki-gun, Ibaraki 311-1393, Japan*

Abstract

Oxygen potential of hypo-stoichiometric $(U_{0.8}La_{0.2})O_{2-x}$ was measured as a function of oxygen-to-metal ratio (2-*x*) at the temperature range from 1173 K to 1473 K. Comparing with uranium oxides doped with other lanthanides, e.g. Lu, Er, Gd and Nd, the relationship between $\Delta\overline{G}_{O_2}$ and the oxygen-to-metal ratio obtained for this sample showed almost the same trend, and for the relatively large oxygen non-stoichiometry *x*, its significance was comparable with that of $(U_{0.8}Gd_{0.2})O_{2-x}$. However, the detail behaviors of $\Delta\overline{H}_{O_2}$ and $\Delta\overline{S}_{O_2}$ were different among these uranium oxides, especially in the near O/M=2.0 region. Furthermore, the oxygen defect structure was evaluated from the relationship between log P_{O_2} and log*x*, and $\Delta\overline{G}_{O_2}$ value of lanthanide-doped uranium oxide was discussed in terms of lanthanide ionic radius.

Keywords: Oxygen potential, lanthanide-doped uranium oxide, oxygen vacancy, ionic radius

[*] Corresponding author
E-mail: arima@nucl.kyushu-u.ac.jp
Tel/Fax: +81-92-802-3494

1. Introduction

Oxygen non-stoichiometric $(U,Ln)O_{2\pm x}$ (Ln: Lanthanide elements) are of particular importance from the viewpoint of evaluation of irradiation behavior of UO_2-based nuclear fuels. Lanthanides have generally high fission yields and form solid solutions with UO_2 over a wide range of Ln contents [1]. This fact requires a systematic database of thermochemial and thermophysical properties for the $(U,Ln)O_{2\pm x}$ in order to evaluate the irradiation behavior. Oxygen potential should be precisely determined prior to the preparation of database since many properties are greatly affected by the oxygen potential via change of oxygen non-stoichiomety x, which is a function of the oxygen potential. For instance, the thermal conductivity, which is one of the most important properties for fuel design, of oxide nuclear fuels has the highest value at the stoichiometry.

Many researchers have investigated oxygen potentials of $(U,Ln)O_{2\pm x}$ with a variety of Ln elements. Une and Oguma [2] have reported a systematic oxygen potential data for $(U,Nd)O_{2\pm x}$. They also measured oxygen potentials of $(U,Gd)O_{2\pm x}$ [3], which is widely used as a high performance light water reactor fuel containing the burnable poison Gd. Oxygen potentials of $(U,Gd)O_{2\pm x}$ were also investigated by many other researchers owing to a technological importance of the $(U,Gd)O_{2\pm x}$ fuel [4]. Lindermer and Brynestad [5] have reviewed oxygen potential data of $(U,Ln)O_{2\pm x}$ with various Ln elements and represented their isotherms of oxygen potentials by using a chemical thermodynamic methods. They reported that there were little different in the oxygen potentials of $(U,Ln)O_{2\pm x}$ with different Ln elements. Osaka et al. [6] have, however, shown that the oxygen potential of $(U,Lu)O_{2-x}$ was notably higher than those of other $(U,Ln)O_{2-x}$. Since high burnup fuels have a variety of lanthanide compositions as fission products according to the fuel specification, such difference in oxygen potential of $(U,Ln)O_{2\pm x}$ should be clarified.

In this study, oxygen potentials of hypo-stoichiometric $(U,La)O_{2-x}$ is experimentally investigated. There are a few data for oxygen potentials of $(U,La)O_{2\pm x}$ [7-9] although the fission yield of La is relatively high. Hagemark and Broli measured the equilibrium oxygen pressures for hyper-stoichiometric $(U,La)O_{2+x}$ with x = 0.01-0.2 [7], and Stadlbauer et al. discussed the thermodynamic parameters of $(U,La)O_{2+x}$ with x = 0.23 [8]. Meanwhile, the oxygen potentials of

hypo-stoichiometric $(U,La)O_{2-x}$ with La = 1 and 5 mol% were measured by Matsui et al. [9]. Therefore, the present results are discussed from various viewpoints; in particular, oxygen non-stoichiometry related defect structures in $(U,La)O_{2-x}$ with La = 20 mol% are focused on. Comparison of effects of La on the oxygen potential with those of other Ln elements is another topic of the present study.

2. Experimental

The sample of $(U_{0.80}La_{0.20})O_{2-x}$ solid solution was prepared by a conventional powder metallurgical method. Appropriate amounts of UO_2 and La_2O_3 powders were weighed and thoroughly mixed in an agate mortar with a pestle in acetone medium. The UO_2 powder was derived from an ammonium diuranate precursor. Then, the mixed powder was pressed at 200 MPa into a pellet by a uniaxial pressing unit. The compacted pellet was heated in He gas at 1673 K for 10 h. The rates of temperature increase and decrease were set to 300 $K \cdot h^{-1}$. The heat-treated pellet was ground, thoroughly mixed and milled again. This sample preparation procedure was repeated once more in order to form a complete solid solution. Temperature and heating time for the second heat-treatments were changed to 1873 K and 4 h, respectively. Then, it was confirmed by a X-ray diffraction measurement that the pellet thus prepared had a single phase solid solution with a fluorite type structure, $(U,La)O_{2-x}$.

The detailed procedure for the oxygen potential measurement was described in the previous papers [10,11]. In brief; the sintered sample (about 200 mg) was made the thermogravimetric measurement with a Rigaku TGA apparatus (model TG-8120) for the determination of oxygen-to-metal (O/M) ratio as a function of oxygen partial pressure, P_{O_2}. The pre-determined temperatures of measurement were 1173 K, 1273 K and 1473 K. The $(U_{0.80}La_{0.20})O_{2-x}$ sample was loaded into an alumina pan and placed in the TGA apparatus. For reference, an alpha-alumina sample was loaded into another alumina pan and also placed in the apparatus. Equilibrium oxygen partial pressure was adjusted in the range from 10^{-22} to 10^{-14} MPa at 1173 K, from 10^{-20} to 10^{-12} MPa at 1273 K and from 10^{-17} to 10^{-9} MPa at 1473 K by changing the ratio of H_2O to H_2 in the Ar flowing gas. The H_2O/H_2 ratio was adjusted by changing the gas flow rate of Ar gas containing 4 % H_2 (Ar/H_2) into the moisture-saturated space above temperature-controlled water in a chamber under the constant total gas flow rate for TGA apparatus. The moisture amount in the chamber space was adjusted by changing the temperature of the water. The H_2 content was also adjusted by mixing Ar/H_2 gas with a pure Ar gas. Equilibrium oxygen partial pressure was measured with a stabilized zirconia oxygen sensor (ST-Lab., model SiOC-200C) at the outlet of the TGA apparatus. The oxygen

sensor was calibrated prior to the TGA using the oxidation reaction of pure chromium metal and a standard gas containing a known amount of oxygen. Small weight changes (Δm ~ μg) in the sample were continuously monitored while changing the P_{O_2} at the pre-determined temperatures step by step. The O/M ratios for various P_{O_2} at pre-determined temperatures were calculated from the weight changes relative to the stoichiometry, O/M = 2.00. The stoichiometry, O/M=2.00, at each temperature was defined as that showing the steep increase of oxygen partial pressure with an increase of the O/M ratio. This definition is appropriate considering the similarity between the La–U–O system and other RE–U–O (RE: Rare-earth) systems [1] which show the steep increase of P_{O_2} around the stoichiometry. Estimated errors of the oxygen potential, which is defined by using Eq. (1) in section 3, and O/M ratio were ±10 kJ/mol and ±0.002, respectively [10].

3. Results and discussion

Fig. 1 shows the measurement data which gives the relationship between $\Delta\overline{G}_{O_2}$ and the O/M ratio of $(U_{0.80}La_{0.20})O_{2-x}$ at 1173 K, 1273 K and 1473 K. And also, these numerical data are listed in Table 1. As already mentioned, the value of $\Delta\overline{G}_{O_2}$ which steeply increased with an increase of O/M ratio corresponded to the O/M = 2.0. We calculated the $\Delta\overline{G}_{O_2}$ and the variation of the O/M ratio according to following formula,

$$\Delta\overline{G}_{O_2} = RT \ln P_{O_2}, \quad (1)$$

$$\Delta(\mathrm{O/M}) = \Delta m \times 2.0 / m_{\mathrm{O}}. \quad (2)$$

Where, P_{O_2} is the ratio of an equilibrium oxygen partial pressure of system to its standard state, 0.101 MPa, m_{O} is mass of oxygen in O/M = 2.0 and Δm is an amount of mass change from the O/M = 2.0. The oxygen potential increases with an increase of the O/M ratio at all temperatures. In addition, the higher the temperature is, the higher the value of $\Delta\overline{G}_{O_2}$ is. This tendency can be found for other form of rare earth-doped UO_2 (RDU).

In Fig. 2, the $\Delta\overline{G}_{O_2}$ values of $(U_{0.80}La_{0.20})O_{2-x}$ measured at 1273 K were compared with those of $(U_{0.80}Lu_{0.20})O_{2-x}$ [6], $(U_{0.80}Gd_{0.20})O_{2-x}$ [4] and $(U_{0.73}Gd_{0.27})O_{2-x}$ [3]. This figure shows that the $\Delta\overline{G}_{O_2}$ values of $(U_{0.80}La_{0.20})O_{2-x}$ are higher than those of $(U_{0.80}Lu_{0.20})O_{2-x}$, and comparable with those of $(U_{0.80}Gd_{0.20})O_{2-x}$ below O/M = 1.994. On the other hand, in Fig. 3, the $\Delta\overline{G}_{O_2}$ values of $(U_{0.80}La_{0.20})O_{2-x}$ obtained at 1473 K were compared with those of $(U_{0.80}Lu_{0.20})O_{2-x}$ [6] and $(U_{0.80}Er_{0.20})O_{2-x}$ [12]. We can find that the $\Delta\overline{G}_{O_2}$ values of $(U_{0.80}La_{0.20})O_{2-x}$ at 1473 K are smaller than other RDU data. The $\Delta\overline{G}_{O_2}$ values of $(U,Nd)O_{2-x}$ [2] were not plotted in these graphs since they are almost the same as those of $(U,Gd)O_{2-x}$ [3]. From the above facts, the effect of La addition to UO_2 on $\Delta\overline{G}_{O_2}$ values seemed to be comparable with that of Gd, and smaller than those of Lu and Er.

Fig. 4 shows the relationships between P_{O_2} and the oxygen non-stoichiometry x, for $(U_{0.80}La_{0.20})O_{2-x}$ at each temperature. It is known that the slope n of $\log P_{O_2}$ versus -log$x$ is an

indicator of the predominant defect structure for non-stoichiometric oxide [13]. The slopes for $(U,La)O_{2-x}$ thus obtained are summarized in Table 2, together with those of $(U,Gd)O_{2-x}$ obtained by other researchers [3,5]. Since the error of *n* value became large as increasing non-stoichiometry *x*, each error of *n* was conservatively estimated to be ±1. In previous studies [3,5], *n* values decreased with an increase of Gd content and temperature. For $(U,La)O_{2-x}$, the value of *n* obtained for near O/M=2.0 region is different from that obtained for other O/M regions. Near the stoichiometric region, the *n* value becomes 2±1 at 1473 K and 3±1 at 1173 K and 1273 K. On the other hand, in large non-stoichiometric regions, the *n* value becomes 7±1 at 1473 K and 5±1 at 1173 K and 1273 K. Une and Oguma proposed the point and cluster defect models for oxygen vacancies in $(U,Gd)O_{2-x}$ [3]. In the former model, oxygen vacancies as point defects are neutral, singly or doubly charged, and the corresponding defect reaction is given as following Kröger-Vink expressions:

$$O_O = V_O + \frac{1}{2}O_2(g)\,, \tag{3}$$

$$O_O = V_O^{\bullet} + e' + \frac{1}{2}O_2(g)\,, \tag{4}$$

$$O_O = V_O^{\bullet\bullet} + 2e' + \frac{1}{2}O_2(g)\,. \tag{5}$$

The oxygen partial pressure dependences expected from these equilibrium states are -l/2, -l/4 and -l/6, respectively. At higher temperature of 1473 K, the defect structure of $(U,La)O_{2-x}$ may be changed from Eq. (5) to Eq. (3) with an increase of the O/M ratio. On the other hand, in the defect cluster model, oxygen vacancies are ordered or paired in a non-stoichiometric solid solution, and they have divalent, trivalent or tetravalent ionic charge with some liberated electrons. The corresponding equilibrium equations of defect formation are given by

$$2O_O = (V_O V_O)^{\bullet\bullet} + 2e' + O_2(g)\,, \tag{6}$$

$$2O_O = (V_O V_O)^{\bullet\bullet\bullet} + 3e' + O_2(g)\,, \tag{7}$$

$$2O_O = (V_O V_O)^{\bullet\bullet\bullet\bullet} + 4e' + O_2(g)\,. \tag{8}$$

According to Eqs.(6-8), the slopes 1/*n* of the plot of $\log P_{O_2}$ against -log*x* become 1/3, 1/4 and 1/5 respectively. Thus, the defect structures of (U,La)O_{2-x} at 1173 K and 1273 K are considered as the vacancy cluster given by Eqs.(6) and (8). Based on the above defect models, higher charged defects (large *n*) generate at larger *x* values, and all cases in Fig. 4 obeys this explanation. It may be a simplistic view, but oxygen vacancies prefer clustering at low temperatures. Comparing with literature data (*n*~3-5) at near O/M = 2.0, obtained ones (*n*~2-3) for (U,La)O_{2-x} seem to be a little smaller. This results from a valence of oxygen vacancy pair and number of liberated electrons in Eqs. (6-8). Arrangement of lanthanide in order of increasing electronegativity is La (1.1) < Nd (1.14) < Gd (1.2) < Er (1.24) < Lu (1.27). Each numbers of parenthesis is, for example, given by Pauling Table [14]. The larger the difference in electronegativity between metal and oxygen is, the higher the ionicity is, which means bonding electrons are strongly attracted to oxygen. Therefore, the small *n* value which means a small number of liberated electrons may be obtained for (U,La)O_{2-x}.

Figs. 5 and 6 show the partial molar enthalpy $\Delta\overline{H}_{O_2}$ and the partial molar entropy $\Delta\overline{S}_{O_2}$ of oxygen in the (U,La)O_{2-x} as a function of O/M ratio, respectively. In theses figures, the literature data was also plotted. The thermodynamic parameters $\Delta\overline{H}_{O_2}$ and $\Delta\overline{S}_{O_2}$ were calculated based on measured $\Delta\overline{G}_{O_2}$ values by following relations:

$$\Delta H_{O_2} = \Delta G_{O_2} + T\Delta S_{O_2}\,, \tag{9}$$

$$\Delta S_{O_2} = -\frac{\partial \Delta G_{O_2}}{\partial T}\,. \tag{10}$$

The $\Delta\overline{H}_{O_2}$ and $\Delta\overline{S}_{O_2}$ values obtained for RDU show the different behavior with the forms of RDU. The absolute values of these thermodynamic parameters of (U,La)O_{2-x} and (U,Lu)O_{2-x} increase with the O/M ratio. On the other hand, the absolute values of $\Delta\overline{H}_{O_2}$ of (U,Gd)O_{2-x} and (U,Nd)O_{2-x}

decrease as the O/M ratio approaches 2.0, and once those of $\Delta\overline{S}_{O_2}$ increase, then decrease as the increase of the O/M ratio. The reason for such behaviors is unclear in this study in spite of the similar defect structure deduced from the slope analysis, it might be caused by a different form in defect structures beyond the stoichiometry. For example, this trend might indicate that in spite of O/M ≤ 2.0, oxygen defects in $(U,Ln)O_{2-x}$ changes from vacancies to interstitials.

According to the characteristics of lanthanide ions with trivalent charge, it is expected that the defect structure of $(U,La)O_{2-x}$ is similar to those of other RDU. However, the behavior of $\Delta\overline{G}_{O_2}$ were different with the form of RDU. The value of $\Delta\overline{G}_{O_2}$ is generally considered to be a stability of the oxygen vacancy in the fluorite solid solution with oxygen hypo-stoichiometry. Thus, in the hypo-stoichiometric range, it could be that at the given O/M ratio, the larger the absolute value of $\Delta\overline{G}_{O_2}$ is, the higher the stability of the oxygen vacancy is. Here, the value of $\Delta\overline{G}_{O_2}$ can be evaluated in terms of the ionic radius of the doped rare-earth ion [15]. Fig. 7 shows the relationship between the $\Delta\overline{G}_{O_2}$ values and ionic radii of rare-earth. However, the $\Delta\overline{G}_{O_2}$ values obtained for the O/M ratio ≤ 1.995 were plotted because the thermodynamic parameters showed the complicated behavior near the O/M = 2.0. Furthermore, the coordination number (CN) is naively assumed to be 6 for rare-earth ions although the ionic radius depends on the CN of surrounding oxygen ions and the O/M ratio. In this figure, the ionic radii of U(IV) and U(V) for CN = 8, which is given for the fluorite structure, are also depicted. Here, the ionic radius of U(V) for CN = 8 was estimated from the data of CN = 6 and 7 [15]. As shown in this figure, the smaller the ionic radius of rare-earth, the higher the $\Delta\overline{G}_{O_2}$ value is. Meanwhile the $\Delta\overline{G}_{O_2}$ value seems to be almost independent of the ionic radius greater than that of Er, especially for the large O/M ratio. In addition, since the O/M value is nearly equal to 2.0 in the hypo-stoichiometric region, the ionic radii of rare-earth ions could be still larger although these values cannot be exactly known. Shannon gives the relationship between ionic radius and CN (Table 3) [15]. For instance, the ionic radius of Gd ion is 0.0938 nm for CN = 6 and that for CN = 8 is 0.1053 nm. As a result, actually all $\Delta\overline{G}_{O_2}$ data in this figure could be given for larger ionic radii of rare-earth. Therefore, $\Delta\overline{G}_{O_2}$ could be higher for the ionic radius of added lanthanide less than that of host cation, i.e. U(IV). Meanwhile, in other cases, $\Delta\overline{G}_{O_2}$ could become

slightly greater with the ionic radius of added lanthanide for small O/M ratios although it could be almost comparable for the large O/M ratio.

4. Conclusions

Oxygen potentials of $(U_{0.8}La_{0.2})O_{2-x}$ with $0.0 < x < 0.04$ were experimentally determined by the thermogravimetric analysis at 1173 K, 1273 K and 1473 K under the oxygen partial pressures of H_2O-H_2 gas equilibria. The $\Delta\overline{G}_{O_2}$ value of $(U_{0.8}La_{0.2})O_{2-x}$ increased with temperature, and its significance was almost comparable with that of $(U_{0.8}Gd_{0.2})O_{2-x}$ for large x values. However, for small x values, $\Delta\overline{H}_{O_2}$ and $\Delta\overline{S}_{O_2}$ behaviors of $(U_{0.8}La_{0.2})O_{2-x}$ were different from those of Gd- and Nd-doped uranium oxides, but similar to that of Lu-doped one. The relationship between $\log P_{O_2}$ and -log$x$ varied with oxygen non-stoichiometry x, rather than temperature for $(U_{0.8}La_{0.2})O_{2-x}$. The $\Delta\overline{G}_{O_2}$ value of lanthanide-doped uranium oxide at 1273 K was almost independent of the ionic radius greater than that of Er.

Acknowledgments

The authors would like to thank K. Tanaka and I. Sato of Japan Atomic Energy Agency for help with the experiments.

References

[1] C. Keller, H. Engerer, L. Leitner, U. Sriyotha, J. Inorg. Nucl. Chem. 31 (1969) 965.

[2] K. Une, M. Oguma, J. Nucl. Mater. 118 (1983) 189.

[3] K. Une, M. Oguma, J. Nucl. Mater. 115 (1983) 84.

[4] T. B. Lindemer, A. L. Sutton, Jr., J. Am. Ceram. Soc. 71 (1988) 553.

[5] T. B. Lindemer, J. Brynestad, J. Am. Ceram. Soc. 69 (1986) 867.

[6] M. Osaka, K. Tanaka, J. Nucl. Mater. 378 (2008) 193.

[7] K. Hagemark, M. Broli, J. Am. Ceram. Soc. 50 (1967) 563.

[8] E. Stadlbauer, U. Wichmann, U. Lott, C. Keller, J. Solid State Chem. 10 (1974) 341.

[9] T. Matsui, K. Naito, J. Nucl. Mater. 138 (1986) 19.

[10] M. Osaka, I. Sato, T. Namekawa, K. Kurosaki, S. Yamanaka, J. Alloys Compd. 397 (2005) 110.

[11] M. Osaka, K. Kurosaki, S. Yamanaka, J. Nucl. Mater. 357 (2006) 69.

[12] H.S. Kim, Y.K. Yoon, M.S. Yang, J. Nucl. Mater. 209 (1994) 286.

[13] O.T. Sørensen, Thermodynamics and defect structure of nonstoichiometric oxides, in: O.T. Sørensen (Ed.), Nonstoichiometric Oxides, Academic, New York, 1981, p. 1.

[14] L. Pauling, The nature of the chemical bond and the structure of molecules and crystals: an introduction to modern structural chemistry, Ithaca, NY, Cornell University Press, 1960.

[15] R.D. Shannon, Acta Cryst. A32 (1976) 751.

Figure captions

Figure 1 Oxygen potentials of $(U_{0.8}La_{0.2})O_{2-x}$ as a function of the oxygen-to-metal ratio at 1173 K, 1273 K and 1473 K.

Figure 2 Comparison of oxygen potentials of $(U_{0.80}La_{0.20})O_{2-x}$ with those of $(U_{0.80}Lu_{0.20})O_{2-x}$ and $(U_{0.80}Gd_{0.20})O_{2-x}$ at 1273 K.

Figure 3 Comparison of oxygen potentials of $(U_{0.80}La_{0.20})O_{2-x}$ with those of $(U_{0.80}Lu_{0.20})O_{2-x}$ and $(U_{0.80}Er_{0.20})O_{2-x}$ at 1473 K.

Figure 4 Relationship between the oxygen partial pressure and the oxygen non-stoichiometry for $(U_{0.80}La_{0.20})O_{2-x}$. Each error of slope *n* was conservatively estimated to be ±1.

Figure 5 Partial molar enthalpy of oxygen for $(U_{0.80}La_{0.20})O_{2-x}$ as a function of oxygen-to-metal ratio, together with those of other lanthanide-doped uranium oxides.

Figure 6 Partial molar entropy of oxygen for $(U_{0.80}La_{0.20})O_{2-x}$ as a function of oxygen-to-metal ratio, together with those of other lanthanide-doped uranium oxides.

Figure 7 Relationship between the oxygen potential of RDU and the ionic radius of doped rare-earth ion at 1273 K. Ionic radii of rare-earth(III) and U(IV and V) ions were obtained for oxygen CN = 6 and 8, respectively. Oxygen potentials of $(U_{0.8}RE_{0.2})O_{2-x}$: RE=Lu [6], Er [12], Gd [4], La (this study) were experimentally obtained. For $(U_{0.8}Nd_{0.2})O_{2-x}$, the plotted values were estimated according to Lindemer's formulation [5].

Table.1 Relationship between oxygen-to-metal (O/M) ratio and oxygen potential of $(U,La)O_{2-x}$

1173 K		1273 K		1473 K	
O/M ratio	$\Delta\overline{G}_{O_2}$ [kJ mol^{-1}]	O/M ratio	$\Delta\overline{G}_{O_2}$ [kJ mol^{-1}]	O/M ratio	$\Delta\overline{G}_{O_2}$ [kJ mol^{-1}]
1.9846	-474.6	1.9794	-472.0	1.9676	-466.1
1.9980	-401.7	1.9970	-396.4	1.9926	-375.3
2.0000	-337.0	2.0000	-326.1	2.0000	-293.5
1.9855	-468.7	1.9804	-467.4	1.9679	-462.5
1.9980	-396.6	1.9977	-392.2	1.9927	-370.5
2.0000	-337.0	2.0000	-324.5	2.0000	-293.5
1.9935	-437.0	1.9819	-461.5	1.9711	-455.4
1.9989	-388.5	1.9977	-385.8	1.9950	-364.1
2.0000	-337.0	2.0000	-322.4	1.9950	-364.2
1.9901	-452.0	1.9877	-445.4	2.0000	-293.4
1.9985	-381.3	1.9984	-377.5	1.9724	-445.8
2.0000	-337.0	2.0000	-322.4	1.9950	-358.3
1.9937	-440.3	1.9954	-413.1	1.9759	-437.2
1.9995	-368.2	2.0000	-317.6	1.9964	-347.7
2.0000	-337.0	1.9968	-387.4	2.0000	-293.5
1.9959	-424.3	2.0000	-318.1	1.9804	-421.5
1.9997	-352.8	1.9891	-434.5	1.9979	-340.1
2.0000	-337.0	1.9992	-356.8	2.0000	-293.5
1.9937	-440.2	2.0000	-315.8	1.9929	-369.1
2.0004	-314.3	1.9836	-458.2	2.0000	-279.3
1.9937	-440.8	1.9978	-380.8	1.9852	-401.0
2.0008	-298.9	2.0000	-320.7	1.9993	-309.2
		1.9954	-415.8	2.0000	-281.8
		2.0016	-294.3	1.9804	-422.6
		1.9872	-447.0	2.0005	-262.4
		1.9989	-369.0		
		2.0000	-316.7		
		1.9954	-411.9		
		2.0004	-305.3		

Table.2 Slope of logarithmic plots of the oxygen partial pressure versus the deviation from stoichiometry for $(U,La)O_{2-x}$ and $(U,Gd)O_{2-x}$

La/Gd fraction	Temperature [K]	Deviation from stoichiometry, x	Slope, n	Reference
La, 0.20	1173	$\geq \sim 10^{-2}$	5±1	This study
	1273		5±1	
	1473		7±1	
La, 0.20	1173	$< \sim 10^{-2}$	3±1	
	1273		3±1	
	1473		2±1	
Gd, 0.14	1273	$< \sim 10^{-2}$	5	Une and Oguma [3]
Gd, 0.14	1573	$< \sim 10^{-2}$	4	
Gd, 0.27	1273	$< \sim 10^{-2}$	4	
Gd, 0.27	1573	$< \sim 10^{-2}$	3	
Gd, 0.20	1273	< ~0.04	5	Lindemer and Sutton [5]
Gd, 0.30	1273	< ~0.05	4	

Table 3 Ionic radii (in nm) as a function of oxygen coordination number (CN) [15]

Ion	Ionic valence	CN		
		6	7	8
La	+3	0.1032	0.11	0.116
Nd	+3	0.0983	0.1046*)	0.1109
Gd	+3	0.0938	0.1	0.1053
Er	+3	0.089	0.0945	0.1004
Lu	+3	0.0861	0.0919*)	0.0977
U	+4	0.089	0.095	0.1
	+5	0.076	0.084	0.092*)

*)Each ionic radius was estimated by those given two other CNs.

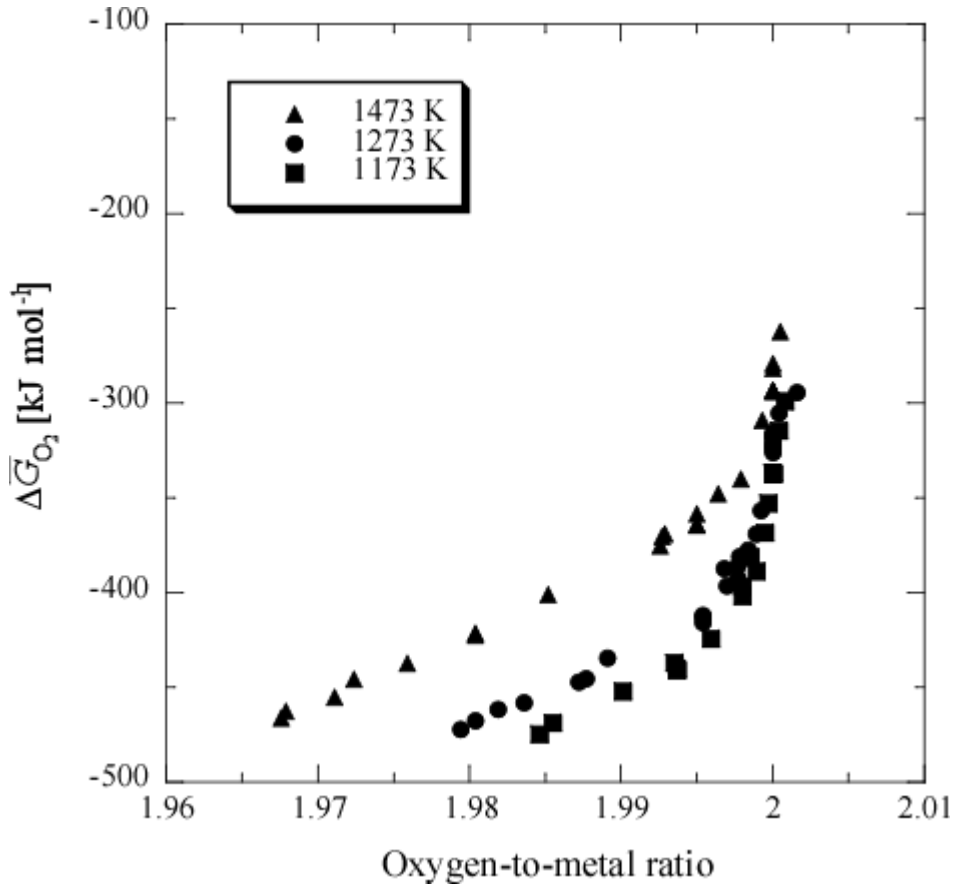

Figure 1 Oxygen potentials of $(U_{0.8}La_{0.2})O_{2-x}$ as a function of the oxygen-to-metal ratio at 1173 K, 1273 K and 1473 K.

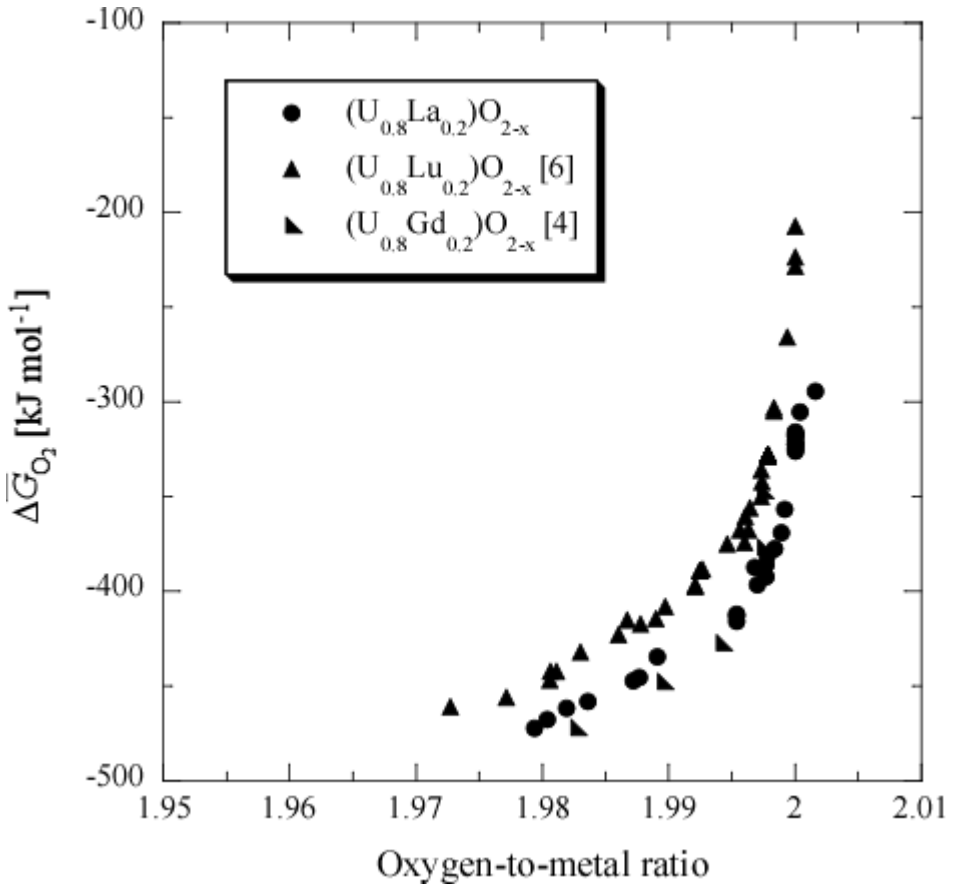

Figure 2 Comparison of oxygen potentials of $(U_{0.80}La_{0.20})O_{2-x}$ with those of $(U_{0.80}Lu_{0.20})O_{2-x}$ and $(U_{0.80}Gd_{0.20})O_{2-x}$ at 1273 K.

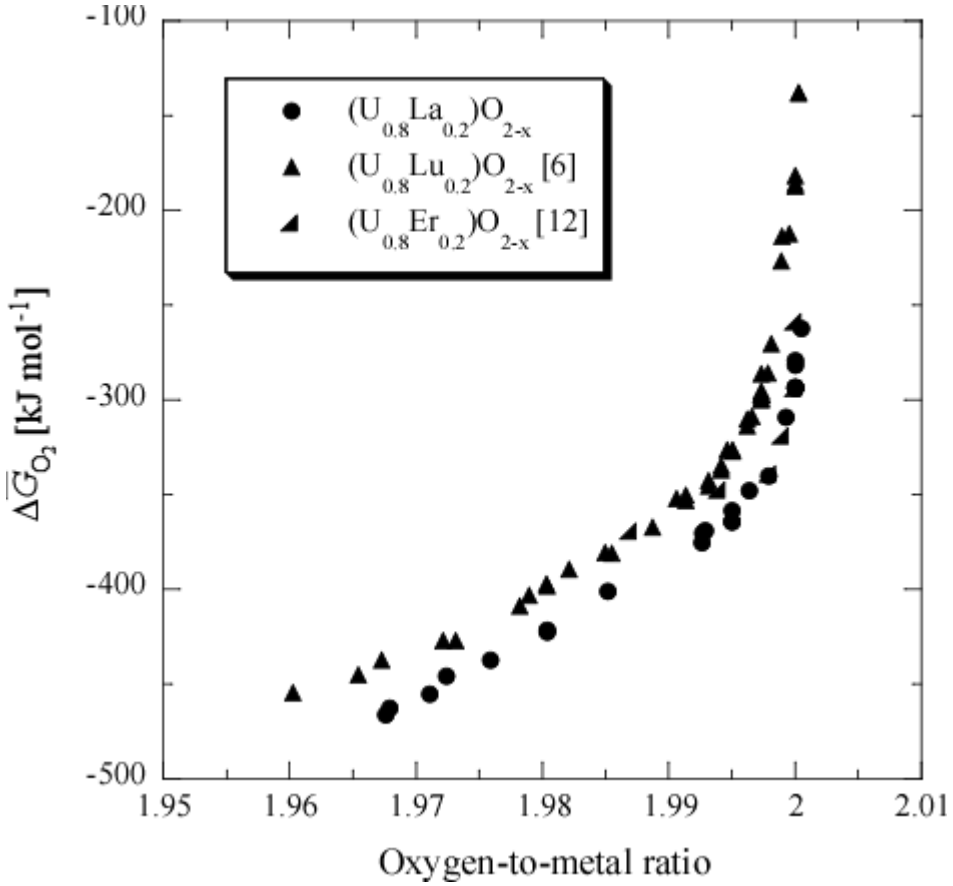

Figure 3 Comparison of oxygen potentials of $(U_{0.80}La_{0.20})O_{2-x}$ with those of $(U_{0.80}Lu_{0.20})O_{2-x}$ and $(U_{0.80}Er_{0.20})O_{2-x}$ at 1473 K.

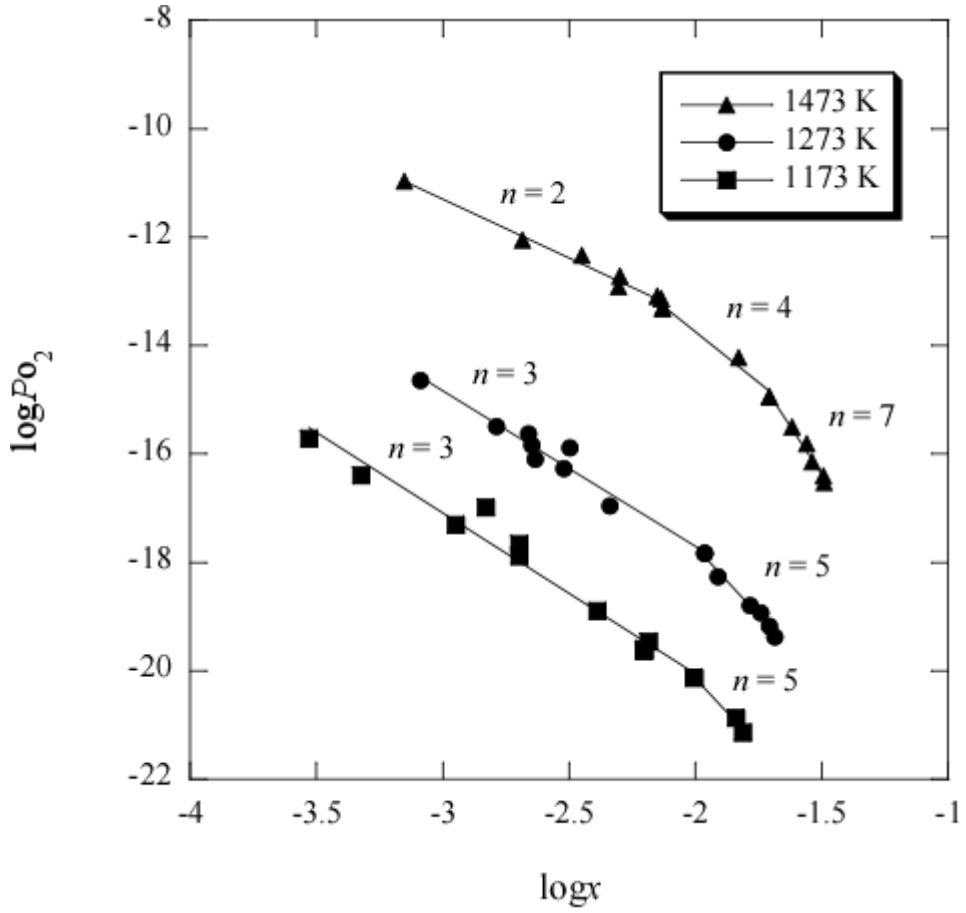

Figure 4 Relationship between the oxygen partial pressure and the oxygen non-stoichiometry for $(U_{0.80}La_{0.20})O_{2-x}$. Each error of slope *n* was conservatively estimated to be ±1.

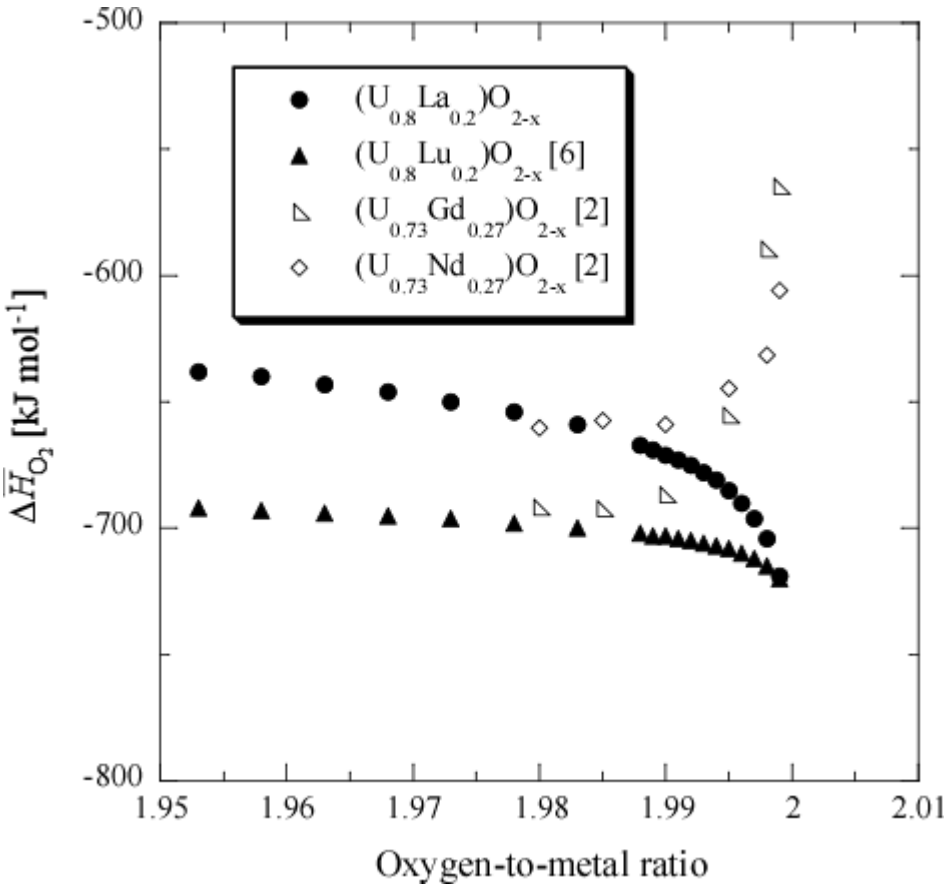

Figure 5 Partial molar enthalpy of oxygen for $(U_{0.80}La_{0.20})O_{2-x}$ as a function of oxygen-to-metal ratio, together with those of other lanthanide-doped uranium oxides.

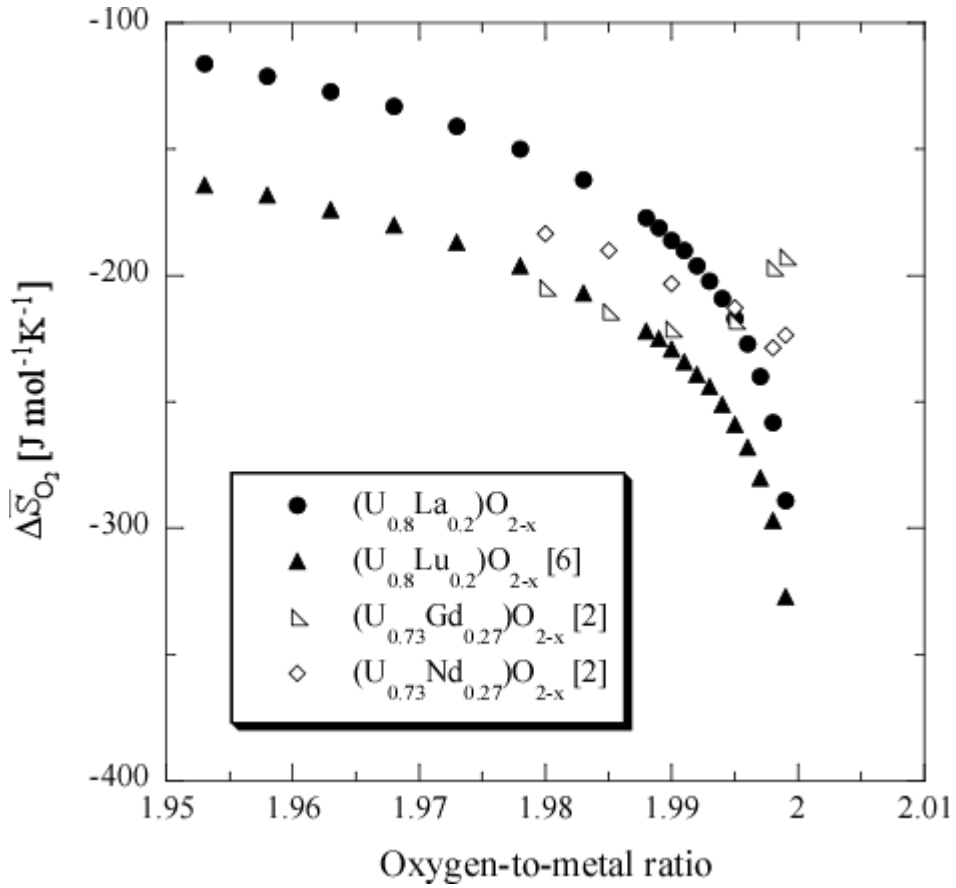

Figure 6 Partial molar entropy of oxygen for $(U_{0.80}La_{0.20})O_{2-x}$ as a function of oxygen-to-metal ratio, together with those of other lanthanide-doped uranium oxides.

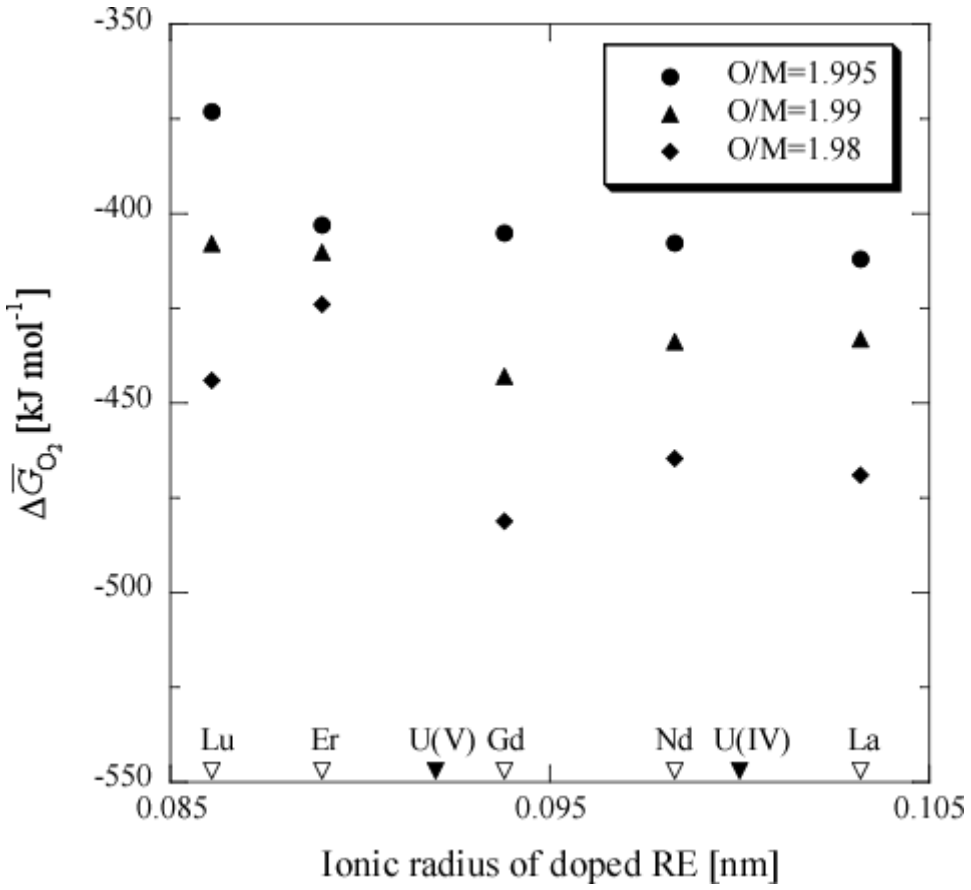

Figure 7 Relationship between the oxygen potential of RDU and the ionic radius of doped rare-earth ion at 1273 K. Ionic radii of rare-earth(III) and U(IV and V) ions were obtained for oxygen CN = 6 and 8, respectively. Oxygen potentials of $(U_{0.8}RE_{0.2})O_{2-x}$: RE=Lu [6], Er [12], Gd [4], La (this study) were experimentally obtained. For $(U_{0.8}Nd_{0.2})O_{2-x}$, the plotted values were estimated according to Lindemer's formulations [5].